ORIGINAL PAPER

Landslide dam failure and flood hydraulics. Part I: experimental investigation

Zhixian Cao · Zhiyuan Yue · Gareth Pender

Abstract Landslide dam failure can trigger catastrophic flooding in the downstream. However, field observation of such flooding is rarely available, while laboratory experimental studies are sparse. The mechanism of landslide dam failure and the flood has so far remained insufficiently understood. Here, we present an experimental investigation of landslide dam failure and the flood. A total of 28 runs of experiments are carried out in a flume of 80 m × 1.2 m × 0.8 m, with differing inflow discharge, dam composition, dam geometry, and initial breach dimension. An array of twelve automatic water-level probes is deployed to measure the stage hydrographs along the flume, and the video recording of the dam failure processes facilitates an estimation of the widening of initial breach. Under the present experimental conditions with dams composed of homogeneous materials, landslide dam failure is primarily caused by erosion of overtopping flow, and lateral mass collapse is also considerable during the cause of breach widening. Cohesive clay may act to mitigate the seepage through the dam and thus its subsidence and appreciably modulate the dam failure process and the flood. However, the impacts of clay may be readily overwhelmed by a large inflow discharge and initial breach. Gravels in the dam may appreciably depress the rate of the dam failure process and thus modify the flood. The present work provides new experimental data set for testing mathematical models of the flood flow due to landslide dam failure.

Keywords Landslide dam · Dam failure · Flood · Erosion · Mass collapse · Flume experiment

Z. Cao (✉)
State Key Laboratory of Water Resources and Hydropower Engineering Science, Wuhan University, Wuhan 430072, China
e-mail: zxcao@whu.edu.cn

Z. Cao · G. Pender
School of the Built Environment, Heriot-Watt University, Edinburgh, UK

Z. Yue
Yangtze River Waterway Research Institute, Wuhan, China

List of symbols

H	Initial dam height (cm)
H_b	Depth of initial breach (cm)
H_d	Initial static water depth at downstream of the dam (cm)
H_f	Maximum residual thickness upon the completion of the dam failure (cm)
H_u	Initial static water depth at upstream of the dam (cm)
Q	Inflow discharge from the far upstream (m^3/s)
S_1, S_2	Initial upstream and downstream slopes of the dam (−)
t	Time (s)
T	Time from the onset to the completion of the dam failure (s)
T_b	Time for the stage in front of the dam to rise up to the peak stage (s)
T_{bg}	Time for the initial breach to grow laterally to the full width of the channel (s)
V	Dam volume (m^3)
W	Initial width of the dam crest (cm)
W_b	Base width of initial breach (cm)

1 Introduction

Natural dams can be generated as a result of climate factors and/or geological processes. Typically, natural dams include landslide dams, which may be generated by earthquakes or heavy rainfall events. The moraine dams of glacier lakes can also be considered as natural dams. Natural dams are usually composed of loose material, hardly consolidated, and may fail by the overtopping flow or through seepage, which can lead to catastrophic flooding in the downstream. Flooding due to landslide dam failure has occurred worldwide (e.g., Costa and Schuster 1988; Cruden et al. 1993, 1997; Bovis and Jakob 2000; Korup 2002; Miller and Cruden 2002; Nicoletti and Parise 2002; Abril and Knight 2004; Dai et al. 2005; Korup and Tweed 2007). Typical examples include the October 1999 case in Poerua River in Westland, South Island, New Zealand (Davies et al. 2007) and the June 1967 case in the Yalong River in China (Li et al. 1986; Chen et al. 1992). Most recently, on May 12, 2008, a major earthquake occurred in Sichuan Province in China, which led to the formation of a series of major landslide dams (e.g., Hu et al. 2009; Cui et al. 2009). One of the largest, the Tangjiashan, landslide dam might fail due to the continuing inflow from the upstream, which could trigger catastrophic flooding in the downstream (the risk was later negated by an artificial spillway channel through the dam). Also, global warming is known to cause glacier retreat, and glacial lakes are formed or expanded, and many glacial-lake outburst flood events have occurred in history (e.g., O'Connor and Baker 1992; Cenderelli and Wohl 2001, 2003; Liu et al. 2003; Shen et al. 2004; Balmfroth et al. 2008, 2009).

A clear understanding of the flooding due to landslide dam failure is certainly necessary for disaster prevention and mitigation. Since real-time in situ measurements of the floods are difficult to make, experiments have been carried out in laboratories, which help enhance the understanding of dam-break hydraulics. However, previous physical experiments are constrained by the comparatively small spatial scales (e.g., Coleman et al. 2002; Chinnarasri et al. 2003; Zhu et al. 2006; Balmfroth et al. 2008, 2009; Schmocker and Hager 2009) and thus may not be able to fully reveal the complicated mechanism of the flood flow. In addition, previous experimental studies have mostly focused on the dam failure process, while the flood hydrographs are sparsely observed. For example, Coleman et al.

(2002) only measured the outflow discharge of the breach, but ignored the flow conditions upstream and downstream of the dam. Chinnarasri et al. (2003), Zhu et al. (2006) and Balmfroth et al. (2008, 2009) did not measure the flow, but the geometry of the failing dam. Indeed, a range of factors involving dam structure and composition as well as hydrodynamic actions may affect the rate and size of breach formation (Morris 2009). In this connection, the experiments by Coleman et al. (2002) and Chinnarasri et al. (2003) are limited to the failure of the dams composed of purely non-cohesive sand under the action of a single inflow discharge. It is certainly critical to understand the influences of the inflow discharge, dam height, and composition on the dam failure and flood processes. Carrivick (2010) tried to conduct experiments of dam break flood over mobile bed in a flume 4 m × 0.5 m × 0.2 m. Yet, there are critical issues open to questions from hydrodynamic perspectives. First, the flow generated by partly raising the lock gate is not dam break flood, rather it is flow under sluice gate, which has been widely investigated in the context of hydraulic engineering. Second, rather coarse sediments (with medium diameters 5, 10 and 15 mm) are used in the experiments, while the flow is very shallow (3–8 cm). The flow depth-to-bed sediment size is far from the real cases in the field, leading to substantially twisted flow structure compared with the field flood. More critically, similitude of sediment movement in the laboratory model and prototype is not considered at all. While field experiments are conducted (e.g., Hoeg 1998; Hoeg et al. 2004), observations of the flood processes are largely hampered because of the risk to damaging the instrumentation and to the personnel and accordingly are normally insufficient for unraveling the mechanism of the dam failure processes. Succinctly, the understanding of the mechanism of landslide dam failure and the flood has so far remained poor and observational data sparse, which constitutes one of the basic impediments to the calibration and testing of mathematical models for the phenomenon.

This paper presents a series of experiments to study landslide dam failure and the flood. The experiments are carried out in a flume of 80 m × 1.2 m × 0.8 m. An array of twelve automatic water-level probes is set at the center of each cross-section along the flume to record the transient stages. Compared with previous experiments on small-scale facilities (e.g., Coleman et al. 2002; Chinnarasri et al. 2003; Zhu et al. 2006; Balmfroth et al. 2008, 2009; Schmocker and Hager 2009), the present experiments cover a wide range of inflow discharges from the upstream, initial dam height, and initial breach dimension. The experimental dams are composed of non-cohesive sand, sand–clay mixture, or sand–gravel mixture. The stage hydrographs and video recordings of the dam failure processes for each run of the experiments are obtained. The data help reveal the mechanisms of dam failure and flood propagation. Use of the experimental data is exemplified in the companion paper on shallow water hydrodynamic modeling of landslide dam failure and flood propagation (Cao et al. 2011). It is noted that dam-break flood, in general, may trigger active sediment transport (debris flow) and bed deformation, which, however, has been addressed elsewhere (e.g., Capart and Young 1998; Cao et al. 2004). Therefore, the present experiments feature a fixed bed initially (i.e., there is no sediment over the channel bed before the onset of the dam failure), and there is no sediment input from the far upstream end. As such, all the sediment involved in the experiments is from the failure of the dam.

2 Experimental setup

The experiments are carried out in a flume, 80 m long, 1.2 m wide, and 0.8 m deep. The flume is made of glass with a fixed bottom slope of 0.001, and the Manning roughness is

approximately 0.012. The experimental setup is illustrated in Fig. 1. The dam is located at 41 m from the inlet of the flume. Twelve automatic water-level probes are mounted at the center of twelve cross-sections (CS1 through CS12), while CS1 is located 19 m from the inlet of the flume. The automatic water-level probes can track transient stages. The tracking speed of the water-level probes is set at 100 mm/s, and the corresponding measurement error is within ±0.5 mm. The sampling frequency is set at 2 Hz. A computer is deployed to process the stage data transmitted from the water-level probes. To facilitate the initialization of the operation of the automatic water-level probes, a 0.15-m-high weir is fixed at the outlet of the flume to keep a small depth of water in the downstream of the dam under the initial condition, and in the upstream of the dam, there is also a similar device around the inlet of the flume to hold some water under the initial condition.

3 Experimental procedure and data

The schematic diagram of the experiments is illustrated in Fig. 2, along with hydraulic and geometric parameters. Prior to the start of a run of experiment, there is some static water up- and downstream the dam, which is necessary for initializing the operation of the water-level probes. As an inflow discharge is facilitated through the inlet of the flume, the water level upstream the dam gradually increases, and once the flow overtops the dam crest, dam failure commences through erosion, i.e., overtopping erosion (dam failure due to seepage is not considered in this study). The initial static water depths immediately upstream and downstream the dam are H_u and H_d: Q is inflow discharge from the upstream; W is the initial width of the dam crest (=20 cm); and H is the initial dam height. In the present work, two different types of dams are considered, respectively, i.e., dams without and with initial breach. For the dam without initial breach, the dam height is uniform across the flume, and the longitudinal profile is illustrated in Fig. 2(a). The initial upstream and downstream slopes of the dam are denoted by S_1 and S_2, respectively. For the dam with initial breach, the initial dam height H is a fixed at 40 cm, a trapezoidal breach is initially set at the center of the dam, of which the depth is H_b, the base width is 4 cm, and the side slope is fixed at 1:1, as illustrated in Fig. 2 (b). Except the initial breach, all the other geometrical conditions of the dam are the same as the dam without initial breach.

Natural landslide dams can be composed of a wide range of sediment sizes, from clay, sand, gravel, and cobble to boulder (Costa and Schuster 1988; Korup 2002). In principle, for hydraulic similitude between the laboratory experiments and the prototype (field) phenomenon, the sediment for the experiments needs to be downsized from that in the
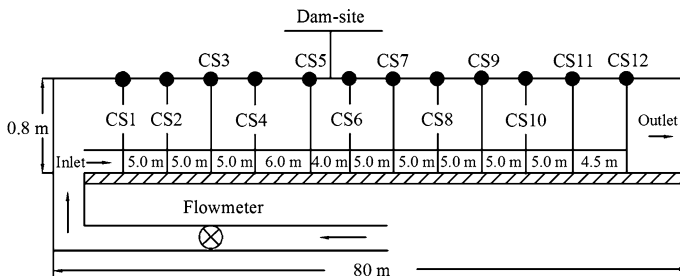

Fig. 1 Experimental setup. Twelve automatic water-level probes are mounted at the center of the flume to track transient stages
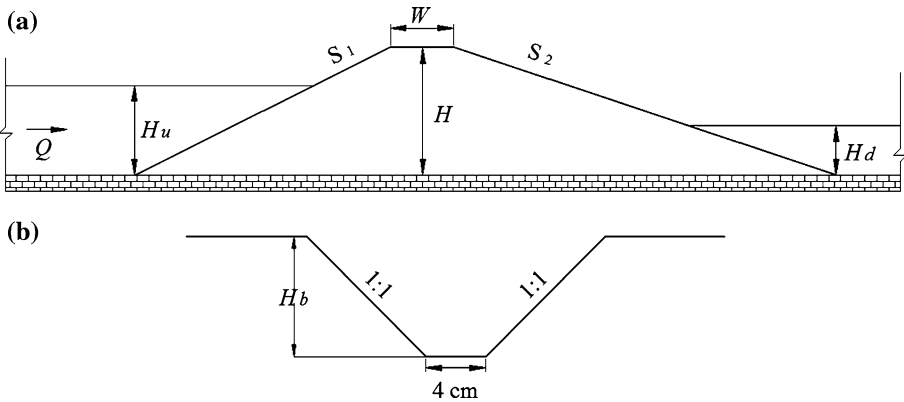
(a)

(b)

Fig. 2 Schematic diagram of dam geometry and hydraulic parameters: **a** longitudinal profile of the dam and **b** dimension of initial breach

field. In the present experiments, the dams are composed of purely non-cohesive sand (SA), a mixture of the sand and cohesive clay (SC) or a mixture of the sand and gravel (SG). The gradation curves of the SA, SC and SG are shown in Fig. 3. The median diameters are 0.8, 0.7, and 1.7 mm, respectively, for the SA, SC, and SG samples, which have a common repose angle of 30° approximately. For the sand–clay mixture (SC), the volume ratio of the clay to the total sand–clay mixture is 25%. While the composition of natural landslide dams can be heterogeneous, it is hard to find a general description of the heterogeneity. Thus, the present experiments are limited to homogeneous dams.

In total, sixteen runs of experiments are conducted for the failure of dams without initial breach (F-Cases) and twelve runs with initial breach (S-Cases), as summarized in Tables 1 and 2, respectively. Here, V is the volume of the dam, H_f is the maximum residual thickness upon the completion of the dam failure, and T_b is the time for the stage in front of the dam to rise up to the peak stage; T is the time from the onset to the end of the dam failure when the erosion of the residual thickness of the dam essentially finishes, which is
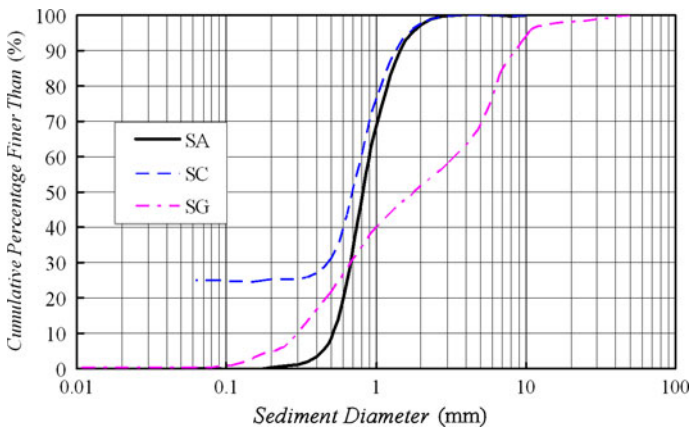

Fig. 3 Gradation curves of dam materials, including non-cohesive sand (SA), sand and cohesive clay (SC), and sand–gravel mixture (SG)

Table 1 Summary of experiments for dams without initial breach

F-Case	S_1, S_2	H (cm)	Q (m^3/s)	V (m^3)	H_u (cm)	H_d (cm)	H_f (cm)	T_b (s)	T (s)	Material
1	1/2, 1/3	15	0.012	0.0855	5.3	5.2	4.4	327	108	SA
2			0.025	0.0855	5.7	4.7	4.0	260	106	
3			0.042	0.0855	5.5	4.6	3.5	127	91	
4		25	0.012	0.2175	5.6	4.1	6.4	842	120	
5			0.025	0.2175	5.5	4.9	6.1	384	113	
6			0.042	0.2175	4.9	4.0	6.3	246	107	
7		40	0.006	0.528	5.4	4.7	8.8	2,793	164	
8			0.012	0.528	5.4	4.5	8.3	1,446	148	
9			0.025	0.528	5.4	4.8	9.7	673	119	
10			0.031	0.528	9.0	7.5	10.0	490	120	
11			0.042	0.528	5.4	4.8	9.0	407	114	
12			0.006	0.528	5.5	4.7	10.5	3,098	257	SC
13			0.012	0.528	5.7	4.4	9.5	1,534	210	
14			0.025	0.528	5.5	4.8	9.0	670	136	
15	1/4, 1/5		0.025	0.528	5.4	4.8	12.8	667	189	SA
16			0.025	0.528	5.4	4.8	17.5	672	262	SG

Table 2 Summary of experiments for dams with initial breach

S-Case	S_1, S_2	H_b (cm)	Q (m^3/s)	H_u (cm)	H_d (cm)	H_f (cm)	T_b (s)	T (s)	T_{bg} (s)	Material
1	1/2, 1/3	4	0.012	5.2	4.5	8.7	1,402	221	129	SA
2			0.025	5.2	5.1	8.3	659	187	99	
3			0.042	5.3	5.0	8.5	397	180	73	
4		10	0.006	6.0	4.2	12.3	2,222	300	253	
5			0.012	6.0	4.0	9.5	1,197	259	194	
6			0.025	5.2	5.6	9.3	555.5	191	136	
7			0.042	5.1	4.6	8.3	370	172	99	
8			0.006	6.0	4.2	12.3	2,267	300	248	SC
9			0.012	6.1	4.1	11.5	1,201	280	180	
10			0.025	5.3	5.4	11.5	553	203	143	
11	1/4, 1/5		0.025	5.2	5.6	12.7	624	300	180	SA
12			0.025	5.2	5.6	15.9	620	306	172	SG

estimated through the video of dam failure process, and T_{bg} is the time for the initial breach to grow laterally to the full width of the channel (breach growth time).

A natural landslide dam may never be uniform across the channel. However, the "idealized" experimental cases for uniform dams are critical for revealing the fundamental mechanism of landslide dam failure and for calibrating and testing mathematical models (Cao et al. 2011). Likewise, the initial breach designed for the experiments (Fig. 2b) is in its geometry rather regular compared with natural landslide dams. Nevertheless, it facilitates easy implementation and is a reasonable surrogate for artificial spillway channels that could be dug out for alleviating downstream flooding under emergency conditions (such as

that in the Tangjiashan Landslide dam following the 2008 major earthquake in Sichuan province, China).

The rate of natural landslide dam failure may vary significantly from case to case. Typically, the failure can last from several days (e.g., the June 1967 case in the Yalong River in China, see Li et al. 1986; Chen et al. 1992) to several years (Korup 2002; Costa and Schuster 1988). The quicker the landslide dam fails, the more severe the downstream flood will be. This study aims to focus on the hydraulics of the flood due to comparatively quick landslide dam failure, which is facilitated by relatively large discharges from the upstream (Tables 1, 2). Physical reasoning suggests that steep-faced dams can fail more easily and therefore generate more severe flood than mildly sloped dams, which is probably why previous experiments (e.g., Schmocker and Hager 2009) have focused on steep-faced dams. The present experiments are designed to be representative of relatively steep-faced dams, with height-to-length (measured along the channel) ratios varying between 1:9.5 and 1:5.5 (Tables 1, 2), which apparently falls within the range of 1:400 to 1:3.3 (Costa and Schuster 1988) of the height-to-length ratio of natural landslide dams.

4 Results and discussions

4.1 General description

Figure 4 shows a sequence of images of the failing dam and the flood flow at different times for F-Case 10. It is seen that the overtopping flow leads to quick failure of the dam, an observation consistent with that of Li et al. (1986), Chen et al. (1992) and Shang et al. (2003). Also, the dam erosion is almost uniform across the flume, which is probably dictated by that fact that the dam crest is initially level and the material is essentially homogeneous laterally. Generally, dam erosion initially occurs at the downstream surface of the dam. As the overtopping flow continuously erodes the dam, the dam top is rapidly lowered, and the downstream slope of the dam gradually becomes milder. It is also observed that the overtopping flow may induce active bed load sediment transport, which occurs essentially uniformly across the channel. For the dam without initial breach under the present experiments, overtopping erosion is indeed the primary factor inducing dam failure, and no substantial mass collapse could be observed. Basically, this observation is applicable to other experimental cases for dams without initial breach (Table 1).

Figure 5 shows a sequence of images of the failing dam at different times for S-Case 6. The dam failure process substantially differs from its counterpart without initial breach (Fig. 4). Here, the dam failure begins within the initial breach, the flow erodes the downstream surface of the dam, and thus, an erosion gully is formed. Then, the gully is deepened gradually by continuous erosion. As the gully becomes progressively deepened and therefore its lateral slopes get steeper, mass lateral collapse of the gully occurs, which leads to gully widening. During this phase of the failure process, both erosion and mass collapse are important. In the later phase, as the initial breach has evolved adequately and the flow has fully overtopped the residual dam, mass collapse becomes less important and erosion overwhelms. For this particular case with a relatively large inflow discharge and also a sufficiently large initial breach (S-Case 6), no laterally full overtopping of the dam was observed before the initial breach is widened to the entire width of the channel. Yet, its occurrence is found in other cases (e.g., S-Case 3) with a comparatively smaller initial breach and differing discharge.
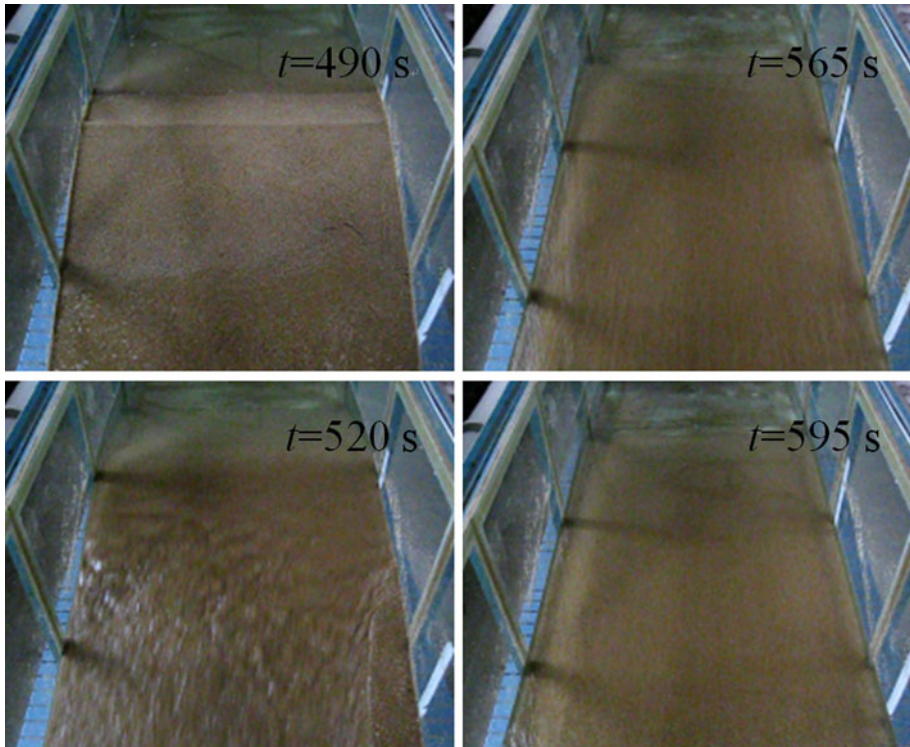
Fig. 4 Images of dam and flow at different times for F-Case 10, showing nearly uniform erosion across the channel. Overtopping erosion is the dominant factor for dam failure without initial breach, and no substantial mass collapse could be observed

Figure 6 shows the measured stage hydrographs at four cross-sections and the degradation of the dam crest for F-Case 10. During the experiments, a ruler is set along the side glass wall of the flume to facilitate the recording of the level of the dam crest. This procedure provides estimated data for the degradation of the dam crest. While being approximate, this observation is rather effective, following Balmfroth et al. (2008). The degradation of the dam crest commences as the flow overtops the dam and ends shortly before the stage hydrographs at distinct cross-sections converge along the flume (Fig. 6).

The stage hydrographs illustrated in Fig. 6 may be divided into three distinct phases. The first phase sees continuous upstream stage rising before the onset of the dam failure, while the downstream stages (CS8 and CS12) remain at the initial static level. The second phase features continuous stage falling and rising respectively up- and downstream of the dam during the dam failure process; the third phase experiences gradual convergence of the upstream and downstream stages following the completion of the dam failure. During the first phase, the back and forth manner of the flood wave propagation is well exemplified in Fig. 6. Specifically, the stages rise asynchronously at differing cross-sections upstream of the dam, due to the continuous inflow from the inlet of the flume. The most upstream cross-section CS1 first sees stage rising and then CS5. Once the flood wave from the inlet reaches the dam, it is reflected by the dam and then propagates upstream, CS5 closest to the dam first experiences the reflected wave and thus stage rising, then CS1. In the second phase, the cross-section (CS5) closest to the dam first experiences the stage falling, followed by
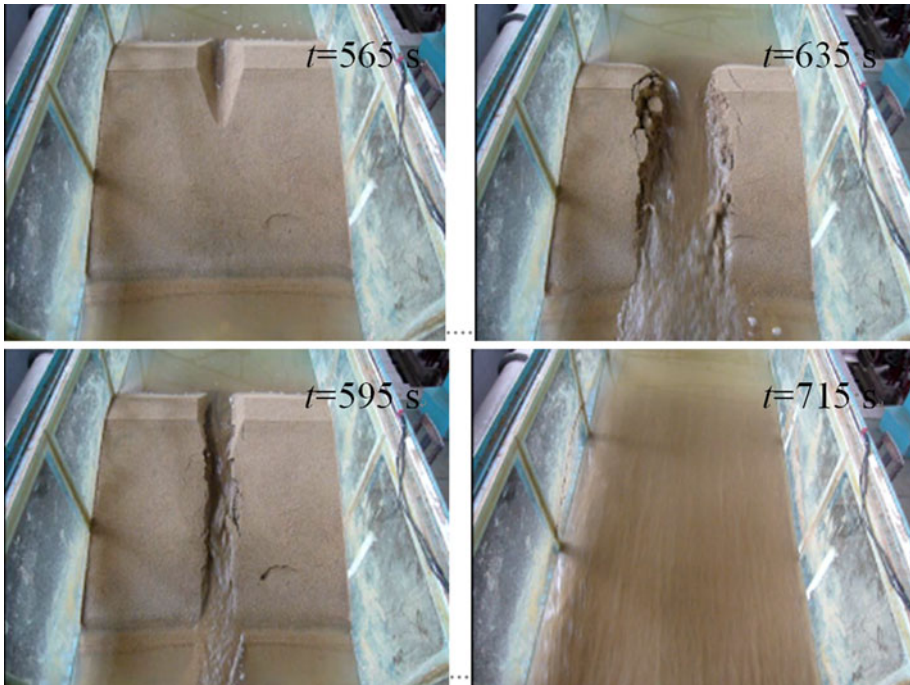
Fig. 5 Images of dam and flow at different times for S-Case 6 with initial breach, showing gully deepening and widening by overtopping erosion and lateral mass collapse
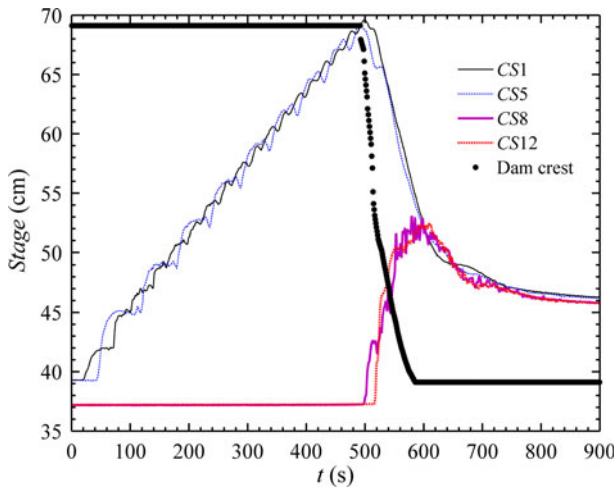

Fig. 6 Typical stage hydrographs and degrading dam crest (F-Case 10). The stage hydrographs can be divided into three distinct phases: the first sees stage rising upstream the dam (CS1 and CS5) prior to the onset of the dam failure, the second features stage falling and rising respectively up- and downstream (CS5 and CS12) the dam, and the third experiences gradual convergence of stages up- and downstream of the dam, following the completion of the dam failure

CS1. At a certain time, the stages at the cross-sections upstream of the dam start to converge. From the onset of the dam failure by overtopping, the downstream stages start to rise, and indeed, the stage at CS8 closest to the dam first rises and then at CS12 as the flood wave propagates toward the far downstream end of the channel. Also, the stages at distinct cross-sections downstream of the dam may reach peaks in a very short period of time, characterizing the highly transient nature of the flood. Following the completion of the dam failure process, in the third phase, the stages at different cross-sections, both up- and downstream of the dam, gradually converge and decline and finally reach a constant state.

In general, the stage hydrographs for all the experimental cases in Tables 1 and 2 qualitatively follow a pattern similar to those shown in Fig. 6. However, the time T_b required for the upstream stage to reach the peak from the initial water level decreases with increasing inflow discharge, as illustrated in Table 1 for F-Cases 7, 8, and 9 and in Table 2 for S-Cases 4, 5, 6, and 7 (with roughly similar initial water levels). Indeed, this can be readily inferred from physical intuition. More importantly, the present experiments demonstrate that the time T from the onset to the end of the dam failure considerably decreases with increasing inflow discharge (F-Cases 7, 8, and 9, and S-Cases 4, 5, 6, and 7). This clearly characterizes the impact of the inflow discharge on the rate of the dam failure process. For a specific reservoir size, the higher the inflow discharge, the quicker the dam fails, and vice versa. From hydrodynamic perspectives, this observation can also be inferred, but has not been revealed in previous experimental studies (Coleman et al. 2002; Chinnarasri et al. 2003). Nevertheless, this understanding is attained under the present experimental conditions (flume), which, however, should not be construed as that other factors (e.g., capacity and irregular plan shape of reservoir) are negligible.

4.2 Influences of initial breach and surface slope

Figure 7 shows the measured stage hydrographs at selected cross-sections for F-Cases 9 and 15 (without initial breach) as well as for S-Cases 6 and 11 (with initial breach). It is shown that the stage upstream the dam without initial breach reaches a higher peak value, and the arrival of the flood in the downstream is appreciably delayed compared with the counterparts for cases with initial breach. Specifically, the arrival of the flood at CS8 (Fig. 7c) was delayed by about 130 s and 70 s when comparing F-Case 9 and S-Case 6, and F-Case 15 and S-Case 11. This is exclusively ascribed to the initial breach, which features a base lower than the crest of the dam. With initial breach, it takes less time for the stage upstream the dam to reach the base level of the initial breach than the dam crest, the failure onsets earlier by the overtopping flow, and consequently, in the upstream, the peak stage is reduced, and in the downstream, the flood arrives sooner than the case without initial breach. Figure 7 also shows that when there is initial breach, the peak stage in the downstream is detectably lower than its counterpart for cases without initial breach, which in principle means mitigated flooding. While the difference in the downstream peak stages for cases without and with initial breach is limited for these particular cases, it can be considerably pronounced at a lower inflow discharge (Fig. 8 for F-Cases 7 and 12 against S-Cases 4 and 8). Further, the impact of initial breach over the stage hydrographs is appreciably attenuated by decreased slopes of the initial dam surface. This can be found in Fig. 7, as the difference between F-Case 15 and S-Case 11 is reduced as compared against that between F-Case 9 and S-Case 6. In general, the differences between the stage hydrographs for dams with and without initial breach (Fig. 7) are qualitatively applicable to other cases (Tables 1, 2).
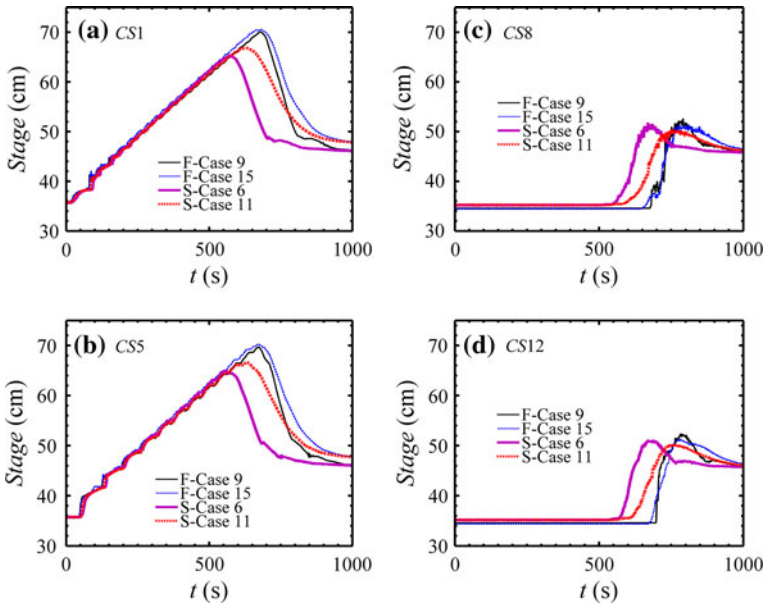
Fig. 7 Stage hydrographs for F-Case 9 and S-Case 6 ($S_1 = 1:2$, $S_2 = 1:3$) as well as for F-Case 15 and S-Case 11 ($S_1 = 1:4$, $S_2 = 1:5$), showing effects of the slopes of initial dam surface as differentiated by initial breach
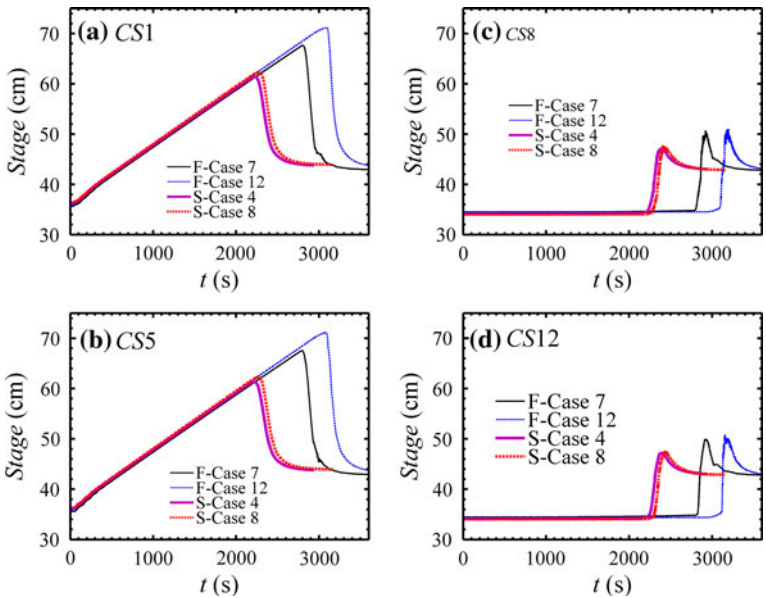

Fig. 8 Stage hydrographs for F-Case 7 and S-Case 4 with non-cohesive sand as well as for F-Case 12 and S-Case 8 with sand–clay mixture, showing that under a relatively low inflow discharge, the effect of clay is substantial when there is no initial breach (F-Cases 7 and 12) and in contrast marginal as overwhelmed by initial breach (S-Cases 4 and 8)

The slopes (S_1 and S_2, Fig. 1(a)) of the initial dam surface may act to modify the failure process. Indeed, this is revealed by the present experiments. When there is no initial breach (F-Cases 9 and 15), reduced slopes of the initial dam surface seem to exhibit stabilizing effects. This is reflected by not only the larger value of the maximum residual thickness H_f (Table 1) for F-Case 15 (than F-Case 9), but the stages. While marginal from the stage hydrographs downstream the dam (CS8 and CS12), the slope effects are appreciable from the stages in the upstream (CS1 and CS5), see Fig. 7. The rate of the declining of the upstream stage for F-Case 15 is lower than F-Case 9, and especially, the final stage of F-Case 15 is a bit higher than F-Case 9. The later observation is not surprising at all from the point of view of open channel hydraulics. After the final phase of the dam failure process, the flow is nearly steady because the inflow discharge is constant, and the flow upstream the dam is entirely controlled by the inflow discharge and the residual thickness. The higher residual thickness for F-Case 15 raises the water level in comparison with F-Case 9. In contrast, downstream the (residual) dam, the discharge is the same as from the upstream, therefore the final stages almost converge for F-Cases 15 and 9 (CS8 and CS12, Fig. 7).

When there is initial breach (S-Cases 6 and 11), the slope effects are qualitatively similar to those under the cases without initial breach (F-Cases 9 and 15), but quantitatively enhanced to a certain extent, as shown in Fig. 7. In particular, because of the stabilizing effects of the milder slopes of S-Case 11, the development of the initial breach is largely hampered (than S-Case 6), the discharge through the dam during this phase is much lower than the inflow discharge, and accordingly, the upstream stage continues to rise over the base level of initial breach after the onset of the failure processes. This is why the peak stage of S-Case 11 upstream the dam (CS1 and CS5) is much higher than its counterpart for S-Case 6 (Fig. 7). This observation appears to characterize the highly complicated nature of the impacts of dam geometry on the failure process.

4.3 Influence of dam composition

When the dam is composed of sand–clay mixture or sand–gravel mixture (Tables 1, 2), the failure process and the stage hydrographs of the flood are qualitatively similar to those for dams of purely non-cohesive sand (Figs. 4, 5, 6). Briefly, under the present experiments, overtopping erosion is the primary factor inducing the dam failure, and lateral mass collapse is also considerable where there is initial breach. Quantitatively, the clay content may appreciably depress the rate of the dam failure process and accordingly increase the total time of the dam failure process, if there is no initial breach. As illustrated in Table 1, the time T from the onset to the completion of the dam failure increases as clay is added to the dam (F-Case 14 versus F-Case 9, F-Case 13 versus F-Case 8, and F-Case 12 versus F-Case 7, Table 1), while other conditions remain unchanged. This observation of the clay effect is more obvious when the inflow discharge is lower. In this connection, the time T evidently decreases with increasing inflow discharge, whether there is clay or not (Tables 1, 2).

Figure 8 shows a comparison between the measured stage hydrographs for F-Cases 7 and 12 as well as for S-Cases 4 and 8. These four cases feature the same inflow discharge from the upstream, 0.006 m³/s, and approximately the same initial water depths, but different dam composition (with or without cohesive clay) and initial dimension of breach (with or without initial breach), see Tables 1 and 2. Figure 8 shows that there is substantial difference between the stage hydrographs for F-Cases 7 and 12 without initial breach, exemplifying the role of clay in modifying the dam failure process and the flood flow. Particularly, the peak stages upstream of the dam for F-Case 7 are considerably lower than

those for F-Case 12 ($\sim$3.5 cm at CS1 and CS5), and the flood wave for F-Case 7 arrives considerably earlier ($\sim$260 s at CS8 and CS12) in the downstream than its counterpart for F-Case 12. Physically, seepage through the dam is inevitable, especially when there is no cohesive clay in the dam (purely non-cohesive sand). While the amount of water loss arising from the seepage may be rather limited compared with the bulk volume of the water in the reservoir, the seepage may lead to substantial dam subsidence prior to the onset of the dam failure by overtopping. This effect can be augmented for those experimental cases with relatively small discharges and high dams (e.g., F-Case 7), because of the longer time needed for the water level in the reservoir to reach the dam crest to initiate overtopping erosion. As the dam is substantially subsided, the onset of the dam failure by overtopping occurs earlier and at an appreciably lower upstream stage, and therefore, the flood wave reaches a downstream cross-section much earlier (Fig. 8). However, when there is initial breach in the dam, the overall difference is largely reduced or simply marginal between the stage hydrographs in relation to dams of purely non-cohesive sand and sand–clay mixture (S-Case 4 versus S-Case 8). Consequently, the impacts of cohesive clay over the dam failure process and the flood are readily overwhelmed by the initial breach.

The impacts of cohesive clay on the dam failure process and the flood can be modified by the inflow discharge from the upstream. Figure 9 shows a comparison between the measured stage hydrographs for F-Cases 9 and 14 as well as for S-Cases 6 and 10. These four cases have the same inflow discharge from the upstream (0.025 m³/s), much higher than those shown in Fig. 8 (0.006 m³/s) and approximately the same initial water depths, but different dam composition (with or without cohesive clay) and initial dimension of breach (with or without initial breach). As shown in Fig. 9, the stage hydrographs between
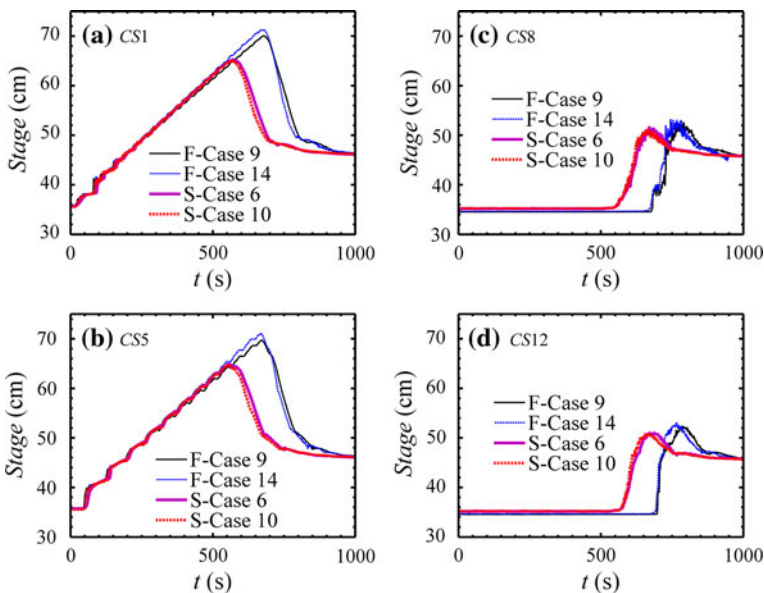

Fig. 9 Stage hydrographs for F-Case 9 and S-Case 6 with non-cohesive sand as well as for F-Case 14 and S-Case 10 with sand–clay mixture, showing that under a comparatively large inflow discharge, the effect of clay is negligible irrespective of whether there is initial breach (S-Cases 6 and 10) or not (F-Cases 9 and 14), as overwhelmed by the inflow
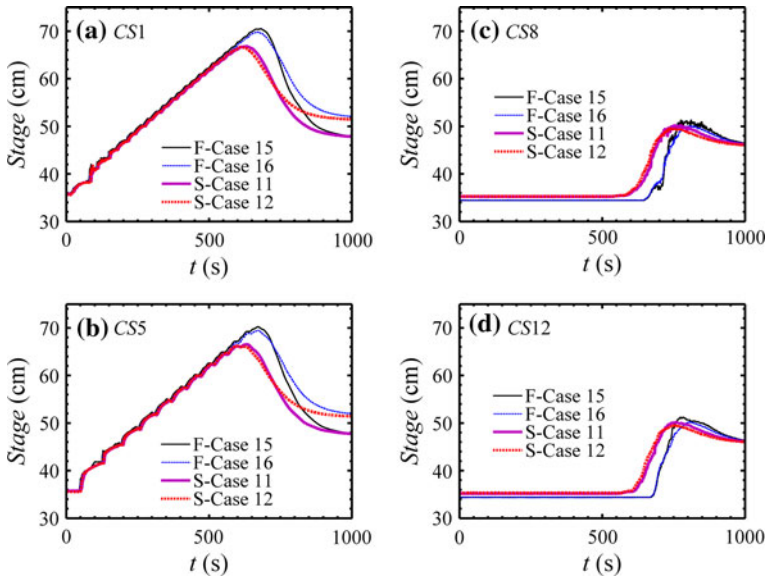
Fig. 10 Stage hydrographs for F-Case 15 and S-Case 11 with non-cohesive sand as well as for F-Case 16 and S-Case 12 with sand–gravel mixture, showing stabilizing effects of gravel, irrespective of whether there is initial breach or not

F-Cases 9 and 14, as well as between S-Cases 6 and 10 exhibit little difference; thus, the effect of clay is overwhelmed by the higher inflow discharge.

Figure 8 also indicates that the initial breach may have substantial impacts on the flood. The downstream peak stages for S-Cases 4 and 8 are much lower than those of F-Cases 7 and 12, respectively (by 2.7 and 3.4 cm at CS12, i.e., by 17.31 and 20.41%). And yet, when the inflow discharge increases, the difference between the downstream peak stages due to initial breach diminishes. As shown in Fig. 9, the downstream peak stages for S-Cases 6 and 10 are lower than those of F-Cases 9 and 14, respectively, by 1.3 and 2.0 cm at CS12 (i.e., by 7.32 and 10.80%). Comparatively, a higher inflow discharge leads to higher peak stages in the downstream, while other conditions remain unchanged. As shown in Figs. 8 and 9, the peak stage at CS12 for F-Case 9 is higher than its counterpart for F-Case 7 by about 2.3 cm (i.e., by 14.74%).

While the difference in the downstream peak stages due to clay, initial breach and inflow discharge is of the order of magnitude of centimeters under the laboratory scales, it may point to considerably varied flooding in the field prototype scale and merits consideration in flood defense design and risk management. The above observations certainly characterize the prime role of the inflow discharge in dictating the dam failure process and the flood, which can overwhelm the impacts of cohesive clay and initial breach.

The impacts of gravel in the dam on the failure process and the flood are substantially different from those of cohesive clay (Figs. 8, 9). Figure 10 shows a comparison between the measured stage hydrographs for F-Case 15 and S-Case 11 with non-cohesive sand as well as for F-Case 16 and S-Case 12 with sand–gravel mixture. Irrespective of whether there is initial breach or not, the gravel exhibits stabilizing effects and therefore affects the flood. The increased maximum residual thickness H_f due to gravel (F-Case 16 versus F-Case 15, S-Case 12 versus S-Case 11) is certainly a manifestation of this effect
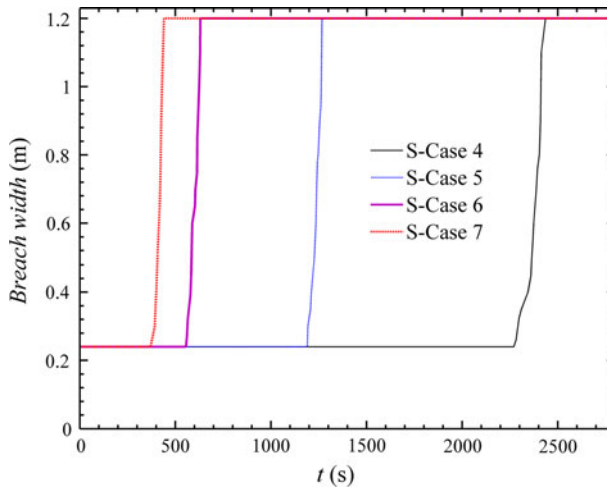
Fig. 11 Breach width growth in time for S-Cases 4, 5, 6, and 7 in relation to differing inflow discharges (Table 2). It is shown that a higher inflow discharge leads to earlier onset of breach widening and quicker breach growth

(Tables 1, 2). Though the difference between the downstream (CS8 and CS12) stage hydrographs is only marginally appreciable for F-Cases 16 and 15 or S-Cases 12 and 11, it is considerable in the upstream (CS1 and CS5), as shown in Fig. 10. Apparently, the rate of the declining of the upstream stage for F-Case 16 and S-Case 12 is respectively lower than F-Case 15 and S-Case 11. Also, the final stage of F-Case 16 is a bit higher than F-Case 15 in the upstream (CS1 and CS5), so is that for S-Case 12 compared with S-Case 11. Not surprisingly, the later observation is actually dictated by a mechanism similar to what leads to the higher final stage in response to reduced slopes of the initial dam surfaces (Fig. 7). More specifically, it is the higher residual thickness of F-Case 16 and S-Case 12 that raises the water level in the upstream, as compared against F-Case 15 and S-Case 11.

Practically, it is interesting to see how quickly the initial breach is widened in response to different inflow discharges. Figure 11 shows the breach width growth in time for S-Cases 4, 5, 6, and 7. All the four cases feature the same dam composition (non-cohesive sand) and initial dam geometry (Table 2). As can be derived from physical reasoning, a high-inflow discharge leads to earlier onset of the breach widening and quicker breach growth and vice versa (Fig. 11). More specifically, the time T_{bg} required for the initial breach to grow laterally to the full width of the channel decreases with increasing inflow discharge (Table 2), as approximately estimated using the video recordings of the dam failure process. Under the present experiments, the impact of dam composition (with clay or gravel) on breach growth is appreciable but minor than that of the inflow discharge, see S-Cases 4, 5, and 6 as compared against S-Cases 8, 9, and 10, respectively, and S-Case 12 in comparison with S-Case 11 (Table 2). Breach widening is further addressed along with computational modeling in the companion paper (Cao et al. 2011).

5 Conclusion

An experimental investigation is presented of landslide dam failure and the flood flow. Under the present experiments, overtopping erosion is the primary mechanism of landslide

dam failure, and lateral mass collapse is also considerable where there is initial breach. This is significant as natural landslide dams are laterally uneven and in cases artificial channels are generated for alleviating the downstream flooding. The inflow discharge dictates the dam failure process and the flood, and the dimension of initial breach is also essential. Milder slopes of the initial dam surface and gravel content in the dam can considerably stabilize the dam, depress the dam failure, and thus affect the flood. Cohesive clay may act to mitigate the seepage through the dam and its subsidence and also appreciably modify the timing of the onset and the rate of the dam failure process. Yet, the impacts of cohesive clay can be readily overwhelmed by a high inflow discharge and initial breach. The observations highlight the vital importance of (a) securing reliable information of the inflow discharge and (b) generating an initial breach of sufficient dimensions for effective management of the downstream flood. The present work provides new observational laboratory data on landslide dam failure and the flood, useful for calibrating and testing mathematical models of the processes.

The mechanism and data of landslide dam failure and the flood attained from this study are inevitably constrained by the spatial and time scales that can be realistically accommodated in the experimental facility. The potential impact of anisotropy of natural dam composition is not yet explored. The impacts of inflow discharge, initial breach, dam geometry, and composition on the flood set within the laboratory scales can be expected to quantitatively amplify in the field prototype scale. In principle, the similitude theory for physical hydraulic modeling (Allen 1952) can be deployed to project the laboratory stage hydrographs to prototype scales, though it needs to exercise due caution, especially when the understanding of sediment transport and mass collapse remains far from complete and the quantification bears uncertainty. This is addressed in the companion paper, as related to mathematical modeling (Cao et al. 2011) that is not subject to scale constraints. While being difficult and even risky to accomplish, field observations of landslide dam failure and the flood will be of significance, especially those that can provide more systematic data than previous studies (Hoeg et al. 2004) for the dam failure and the flood stages in a sufficiently long reach.

References

Abril B, Knight D (2004) Stabilising the Paute river in Ecuador. Civ Eng Proc Inst Civ Eng 157(1):32–38

Allen J (1952) Scale models in hydraulic engineering. Longman, London

Balmforth NJ, Hardenberg J, von Provenzale A, Zammett R (2008) Dam breaking by wave-induced erosional incision. J Geophys Res 113(F01020). doi:10.1029/2007JF000756

Balmforth NJ, von Hardenberg J, Zammett R (2009) Dam-breaking seiches. J Fluid Mech 628:1–21

Bovis M, Jakob M (2000) The July, 1998, debris flow and landslide dam at Capricorn Creek, Mount Meager Volcanic Complex, southern Coast Mountains, British Columbia. Can J Earth Sci 37(10):1321–1334

Cao ZX, Pender G, Wallis S, Carling P (2004) Computational dam-break hydraulics over erodible sediment bed. ASCE J Hydraul Eng 130(7):689–703

Cao ZX, Yue ZY, Pender G (2011) Landslide dam failure and flood hydraulics. Part II: coupled mathematical modelling. Nat Hazards. doi:10.1007/s11069-011-9815-7

Capart H, Young DL (1998) Formation of a jump by the dam-break wave over a granular bed. J Fluid Mech 372:165–187

Carrivick JL (2010) Dam break-outburst flood propagation and transient hydraulics: a geosciences perspective. J Hydrol 380(3–4):338–355

Cenderelli DA, Wohl EE (2001) Peak discharge estimates of glacial-lake outburst floods and 'normal' climatic floods in the Mount Everest region, Nepal. Geomorphology 40(1–2):57–90

Cenderelli DA, Wohl EE (2003) Flow hydraulics and geomorphic effects of glacial-lake outburst floods in the Mount Everest region, Nepal. Earth Surf Process Landf 28(4):385–407

Chen YJ, Zhou F, Feng Y, Xia YC (1992) Breach of a naturally embanked dam on Yalong River. Can J Civ Eng 19(5):811–818

Chinnarasri C, Tingsanchali T, Weesakul S, Wongwises S (2003) Flow patterns and damage of dike overtopping. Int J Sed Res 18(4):301–309

Coleman SE, Andrews DP, Webby MG (2002) Overtopping breaching of noncohesive homogeneous embankments. ASCE J Hydraul Eng 128(9):829–838

Costa JE, Schuster RL (1988) The formation and failure of natural dams. Geol Soc Am Bull 100(7):1054–1068

Cruden DM, Keegan TR, Thomson S (1993) The landslide dam on the Saddle River near Rycroft, Alberta. Can Geotech J 30(6):1003–1015

Cruden DM, Lu ZY, Thomson S (1997) The 1939 Montagneuse River landslide, Alberta. Can Geotech J 34(5):799–810

Cui P, Zhu Y, Han Y, Chen X, Zhuang J (2009) The 12 May Wenchuan earthquake-induced landslide lakes: distribution and preliminary risk evaluation. Landslides 6(3):209–223

Dai FC, Lee CF, Deng JH, Tham LG (2005) The 1786 earthquake-triggered landslide dam and subsequent dam-break flood on the Dadu River, southwestern China. Geomorphology 65(3–4):205–221

Davies TR, Manville V, Kunz M, Donadini L (2007) Modeling landslide dam break flood magnitudes: case study. ASCE J Hydraul Eng 133(7):713–720

Hoeg K (1998) New dam safety legislation and the use of risk analysis. Int J Hydrop Dams 5(5):85–89

Hoeg K, Lovoll A, Vaskinn KA (2004) Stability and breaching of embankment dams: field tests on 6 m high dams. Int J Hydropower Dams 11(1):88–92

Hu XW, Lu XP, Huang RQ, Shi YB, Liu J, Li YB (2009) Developmental features and evaluation of blocking dangers of Dashui ditch debris flow in Tangjiashan dammed lake. Chin J Rock Mech Eng 28(4):850–858

Korup K (2002) Recent research on landslide dams - a literature review with special attention to New Zealand. Progress Phys Geogr 26(2):206–235

Korup K, Tweed F (2007) Ice, moraine, and landslide dams in mountainous terrain. Quat Sci Rev 26(25–28):3406–3422

Li TC, Schuster RL, Wu JS (1986) Landslide dams in south-central China. In: Schuster R (ed) Landslide dams: processes, risk and mitigation. Geotechnical Special Publication No. 3, ASCE, pp 146–162

Liu SZ, Li HX, Yan Y, Chai ZX, Du SP (2003) Assessment of bursting hazards of the ice lakes in Luozha County, Tibet. J Mt Sci 21:128–132

Miller BGN, Cruden DM (2002) The Eureka River landslide and dam, Peace River Lowlands, Alberta. Can Geotech J 39(4):863–878

Morris M (2009) Breaching processes: a state of art review. FLOODsite Project Report T06-06-03. FLOODsite, www.floodsite.net

Nicoletti PG, Parise M (2002) Seven landslide dams of old seismic origin in southeastern Sicily (Italy). Geomorphology 46(3–4):203–222

O'Connor JE, Baker VR (1992) Magnitudes and implications of peak discharges from glacial lake Missoula. Geol Soc Am 104(3):267–279

Shang YJ, Yang ZF, Li LH, Liu DA, Liao QL, Wang YC (2003) A super-large landslide in Tibet in 2000: background, occurrence, disaster and origin. Geomorphology 54(3–4):225–243

Shen YP, Ding YJ, Liu SY, Wang SD (2004) An increasing glacial lake outburst flood in Yarkant River, Karakorum in past ten years. J Glaciol Geocryol 26(2):117

Zhu YH, Visser PJ, Vrijling JK (2006) Laboratory observations of embankment breaching. In: Proceeding of the 7th ICHE congress, September, Philadelphia, USA